SUPPLEMENTARY INFORMATION

SUPPLEMENTARY FIGURES AND LEGENDS

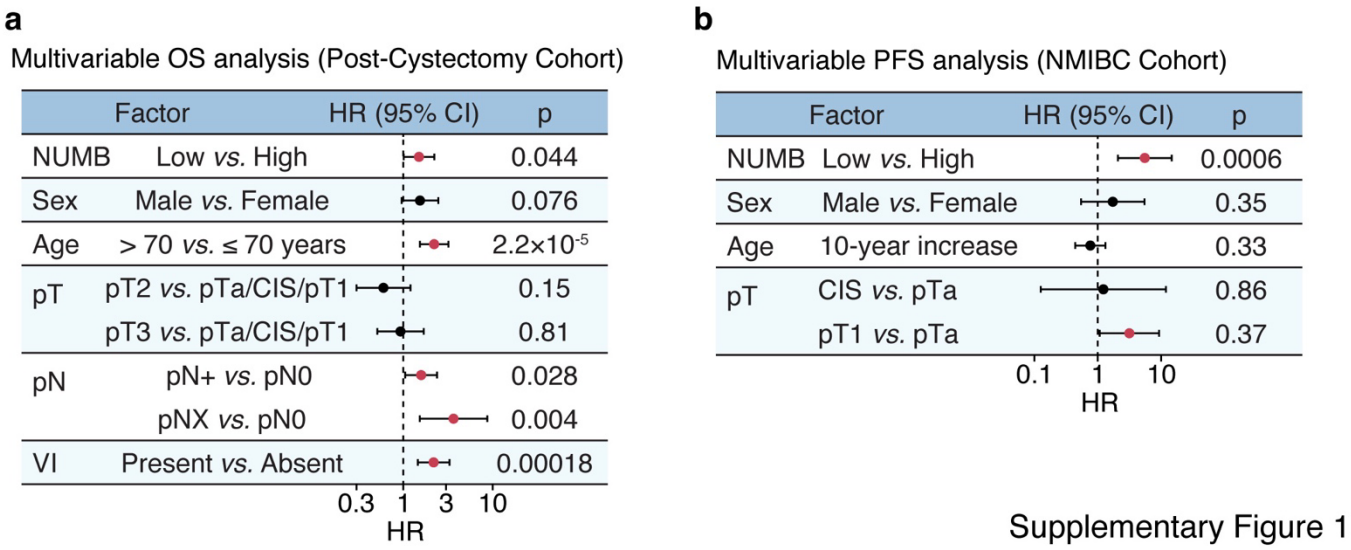

Supplementary Figure 1

Supplementary Figure 1. NUMB is a prognostic biomarker of unfavorable disease course in real-life post-cystectomy and NMIBC patients. a. Multivariable survival analysis of the association between the indicated factors and good (HR<1) or poor (HR>1) prognosis in 258 patients with available follow-up from the post-cystectomy cohort in Supplementary Table 1. Significant associations are marked in red. HR, multivariable hazard ratios with 95% confidence intervals (CI) by Cox proportional hazards model in this and other relevant panels in the figure. p, two-sided Wald-test p-value. **b.** Multivariable progression-free survival (PFS) analysis of the association between the indicated factors and good (HR<1) or poor (HR>1) prognosis in the 77 NMIBC patient cohort from Supplementary Table 2. p, two-sided Wald-test p-value. Source data are provided as Source Data file.

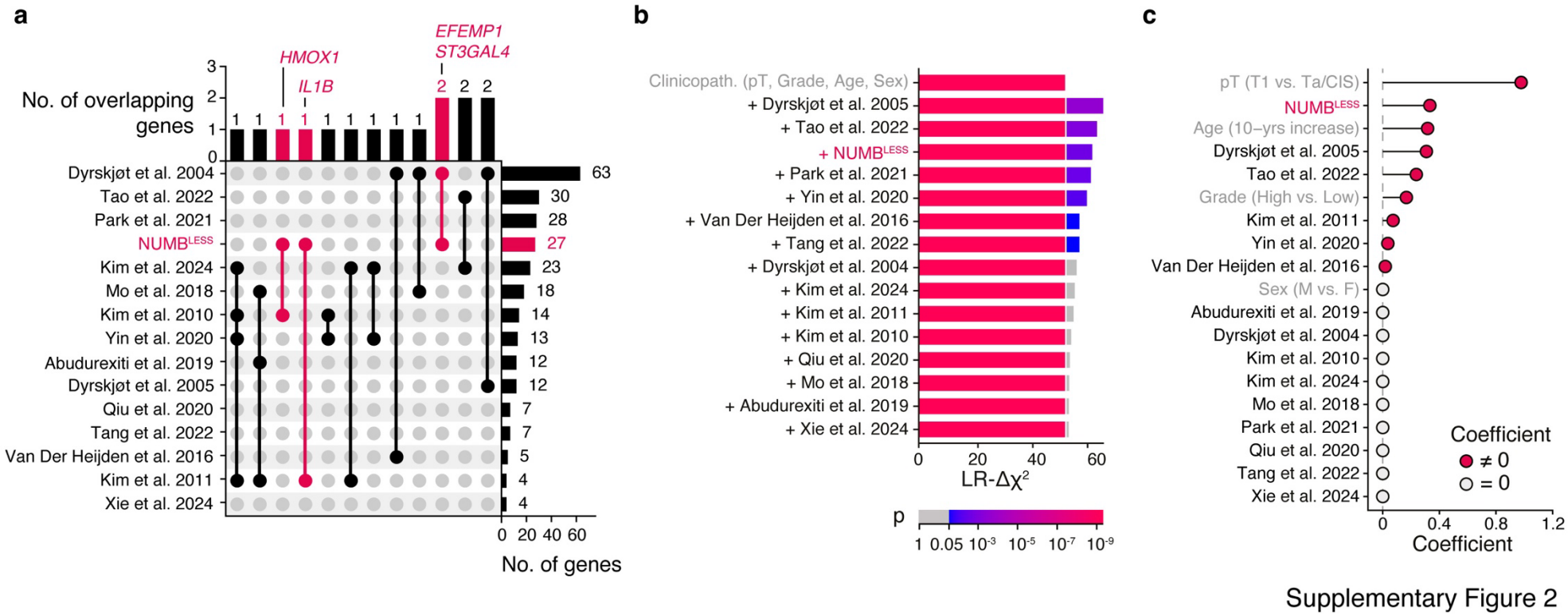

Supplementary Figure 2

Supplementary Figure 2. Comparison of the NUMB^{LESS} signature with other BCa-specific prognostic signatures in NMIBC patients. a. Overlap of genes in the NUMB^{LESS} (indicated in red) and other 14 gene signatures developed for prognostic prediction in BCa (black). The horizontal bar graph on the right represents the total number of genes in each signature. The vertical bar graph at the top shows the number of genes shared between individual signatures, as indicated by the connected dots below the bars. **b.** Prognostic information provided by each BCa gene signature in addition to standard clinicopathological parameters (pT, Grade, Age, Sex, indicated in grey) for risk of progression to MIBC in the NMIBC (UROMOL) cohort (n=535). LR-$\Delta\chi^2$, likelihood ratio values; p, two-sided log-rank test p-value. **c.** Coefficients from a Lasso penalized multivariable Cox proportional hazard model in the NMIBC (UROMOL) cohort (n=535), comparing the redundancy of 15 BCa-specific gene signatures in providing additional prognostic information over standard clinicopathological parameters (grey). The coefficients indicate the relative impact of each variable on the hazard ratio for progression to MIBC. Variables with a coefficient equal to 0 (white) provide no additional contribution to the other variables in the prognostic model. Source data are provided as Source Data file.

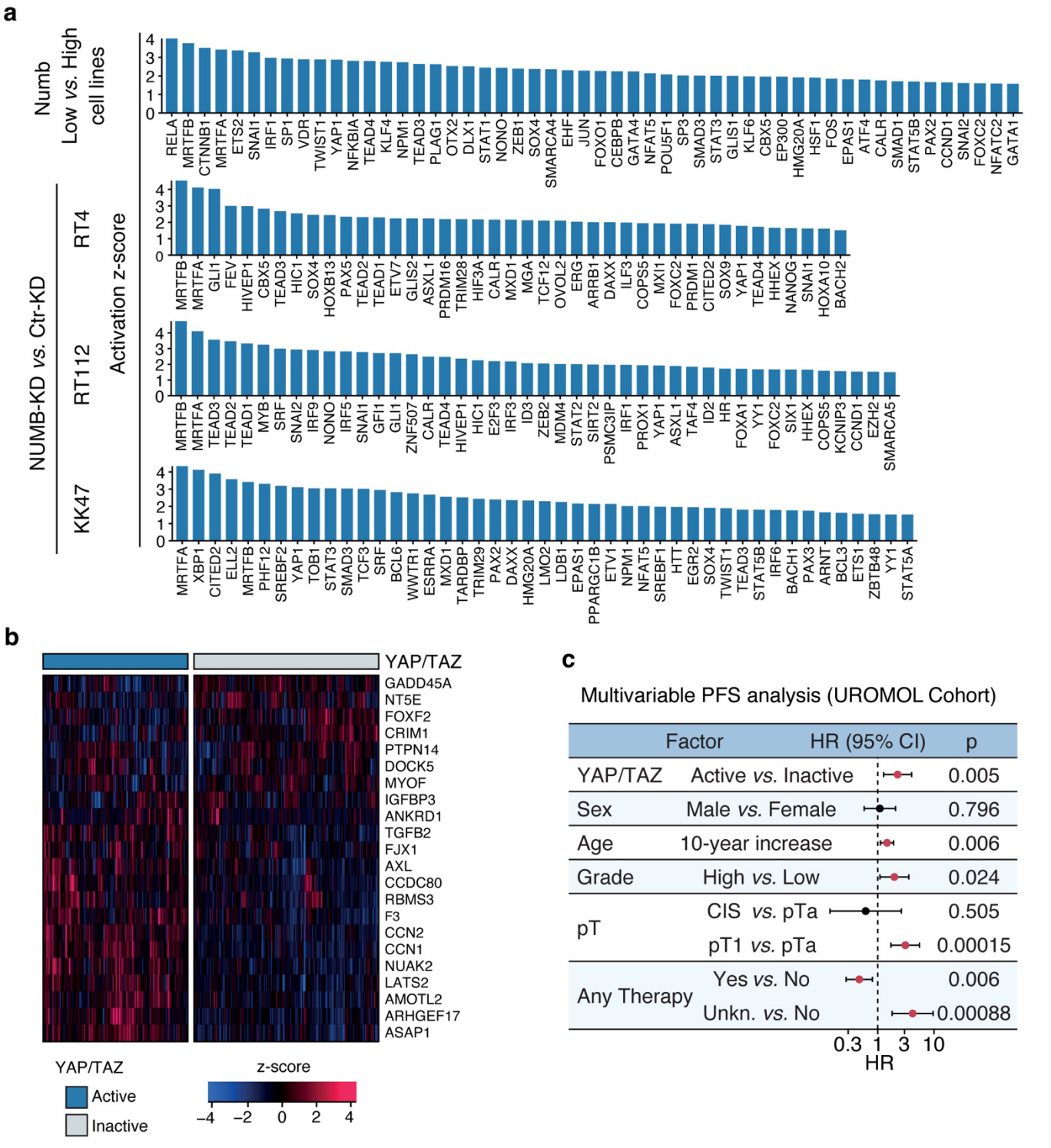

Supplementary Figure 3

Supplementary Figure 3. Relevance of YAP activation status identified in NUMB-deficient preclinical human BCa cell models to NMIBC patients. a. Transcriptional regulators predicted to be activated in MIBC $NUMB^{Low}$ (HT1376, CLS439, 5637) *vs.* NMIBC $NUMB^{High}$ BCa (KK47, RT4, RT112) cell lines (top) and in RT4, RT112 and KK47 NUMB-KD *vs.* Ctr-KD cells (bottom). p-value of overlap <0.05 by one-sided Fisher's exact test. Activation z-score > 1.5. **b.** Heatmap showing the unsupervised clustering of 535 NMIBC tumors from the UROMOL cohort, classified as YAP/TAZ active or inactive, based on the expression levels of 22 genes of the YAP/TAZ signature. **c.** Multivariable progression-free survival (PFS) analysis of the association between the indicated factors and good (HR<1) or poor (HR>1) prognosis in 535 NMIBC patients from the UROMOL cohort. Significant associations are marked in red. HR, multivariable hazard ratios with error bars representing 95% confidence intervals (CI) by Cox proportional hazards model; p, two-sided Wald-test p-value. **d.** Progression-free survival of NMIBC patients of the UROMOL cohort (n=535) who had or had not received BCG, stratified by the 22-gene YAP/TAZ signature into YAP/TAZ active and inactive groups. HR, hazard ratio (95% confidence interval); p, two-sided log-rank test p-value; n, patient number; in this and all other relevant panels. **e.** Same analysis as in 'd' for patients stratified with the $NUMB^{LESS}$ signature into $NUMB^{LESS}$-Like and $NUMB^{LESS}$-Not-Like groups, corresponding to a NUMB-deficient or NUMB-proficient status, respectively. Source data are provided as Source Data file.

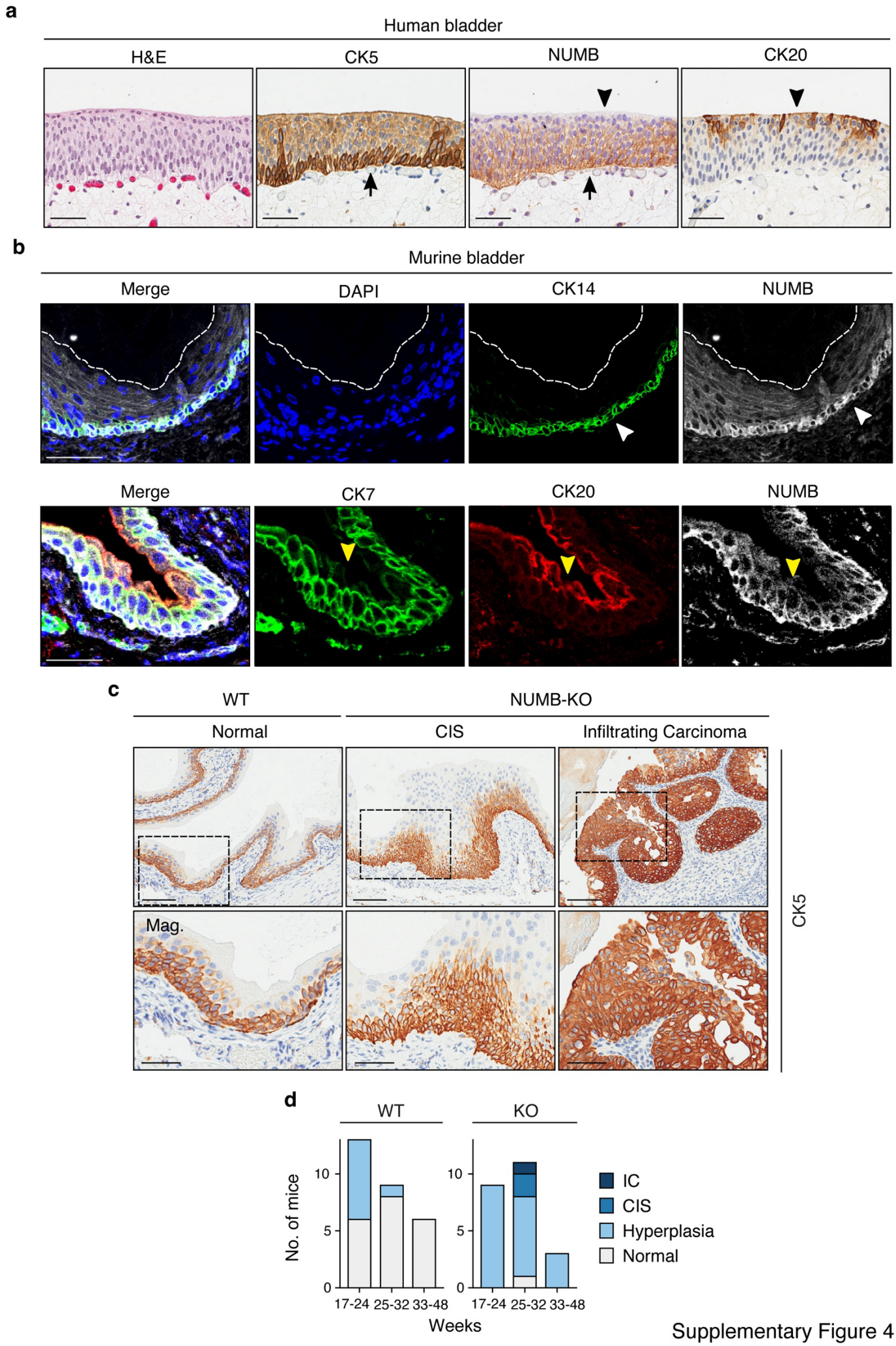

Supplementary Figure 4

Supplementary Figure 4. Characterization of the pro-tumorigenic role of NUMB loss in the NUMB-KO mouse model. a. Representative IHC images of the expression of endogenous NUMB in the normal human urothelium, showing its association with the basal layer. CK5 is a marker for the basal/myoepithelial layer (arrows); CK20 is a marker for superficial cells (arrowheads). Bars, 50 μm. **b**. Representative confocal fluorescence images of FFPE sections of murine bladder. Upper panels show co-staining for endogenous NUMB (white), the CK14 basal/myoepithelial layer marker (green) and DAPI (blue). White arrowheads indicate the basal layer. Lower panels show co-staining for NUMB (white), the intermediate layer marker CK7 (green), and the superficial/umbrella cell marker CK20 (yellow arrowheads). The dashed line delineates the superficial layer of the urothelium. Bars, 50 μm. **c**. Upper panels, representative IHC images of CK5 expression in bladder tissue from NUMB-KO and WT mice showing expansion of basal cells (CK5+) in NUMB-KO lesions (CIS and infiltrating cancer) compared with WT. Boxed areas are magnified (Mag.) in the lower panels. Bars, 100 μm; Mag., 50 μm. **d.** Histopathological phenotypes detected in the urothelium of WT (n=28) and NUMB-KO (n=23) mice sacrificed at different ages. Source data are provided as Source Data file.

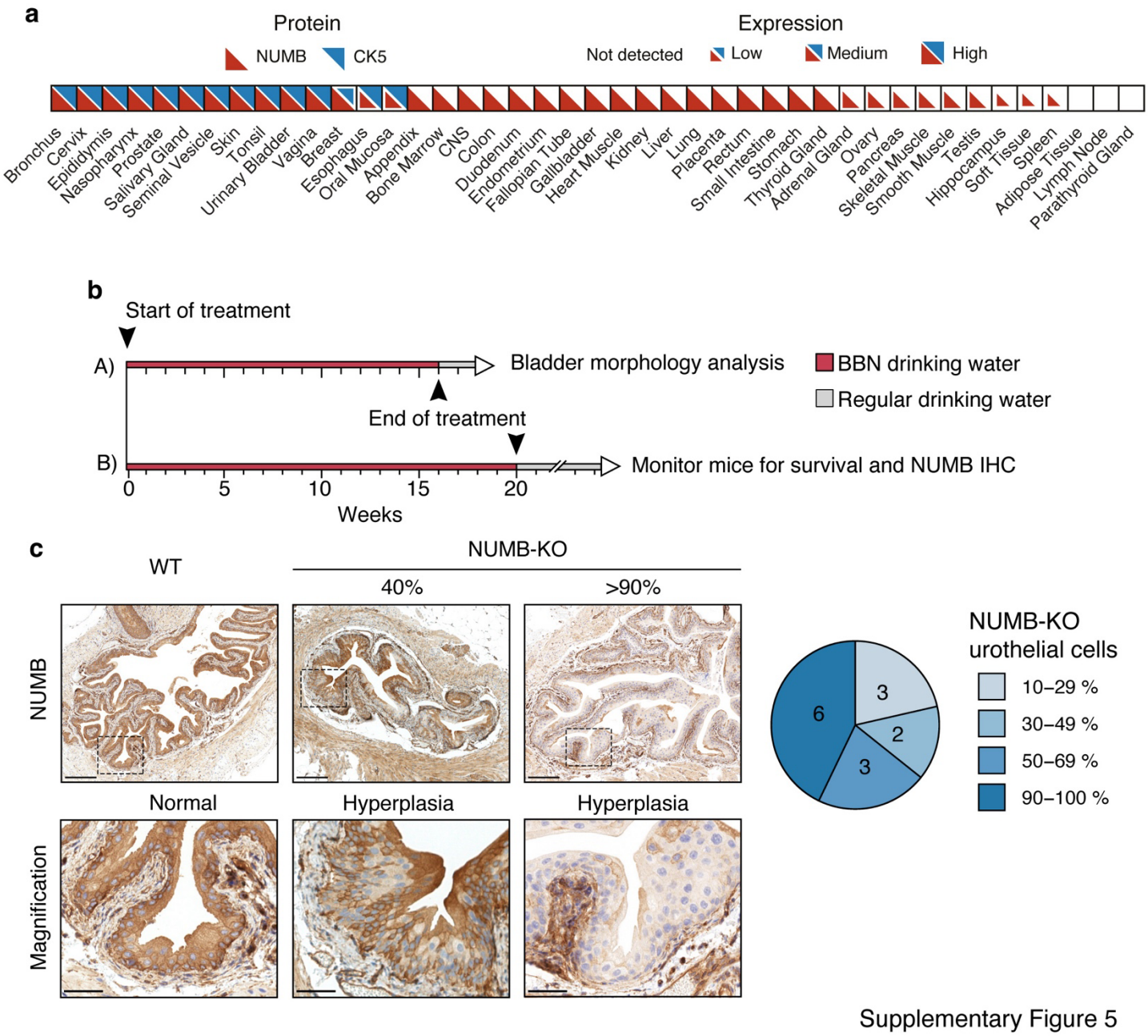

Supplementary Figure 5. Characterization of the NUMB-KO mouse model. a. Protein expression levels of NUMB and CK5 in different tissues according to the human protein atlas. **b.** BBN treatment protocols for 6-8 week old WT *vs.* NUMB-KO mice. A) For the analysis of the incidence of hyperplastic, not-infiltrating CIS and infiltrating cancer lesions in the WT *vs.* NUMB-KO bladder mucosa (shown in Fig. 3c), mice were administered 0.05% BBN in drinking water continuously for 16 weeks and then switched to regular drinking water. Mice were sacrificed two weeks after ending BBN treatment. B) For survival and histological analyses (shown in Fig. 3d-f), mice were administered 0.05% BBN in drinking water continuously for 20 weeks to induce the formation of infiltrating tumors, and then switched to regular drinking water. Mice were monitored for survival

until the experimental endpoint, at which time all surviving mice were sacrificed. Bladder tissues were subjected to IHC analysis of NUMB expression. **c.** Left, representative IHC images of NUMB showing the efficiency of NUMB knock out in the bladder of *Numb*$^{lox/lox}$ *Ck5-CRE* mice sacrificed at 6-8 weeks of age, compared to NUMB expression in the normal urothelium (WT). Magnifications of the boxed areas are shown in the lower panels. Bar, 200 μm; Magnification, 50 μm. Right, pie chart showing the percentage of NUMB-KO urothelial cells in the group of analyzed *Numb*$^{lox/lox}$ *Ck5-CRE* mice (n=14). Source data are provided as Source Data file.

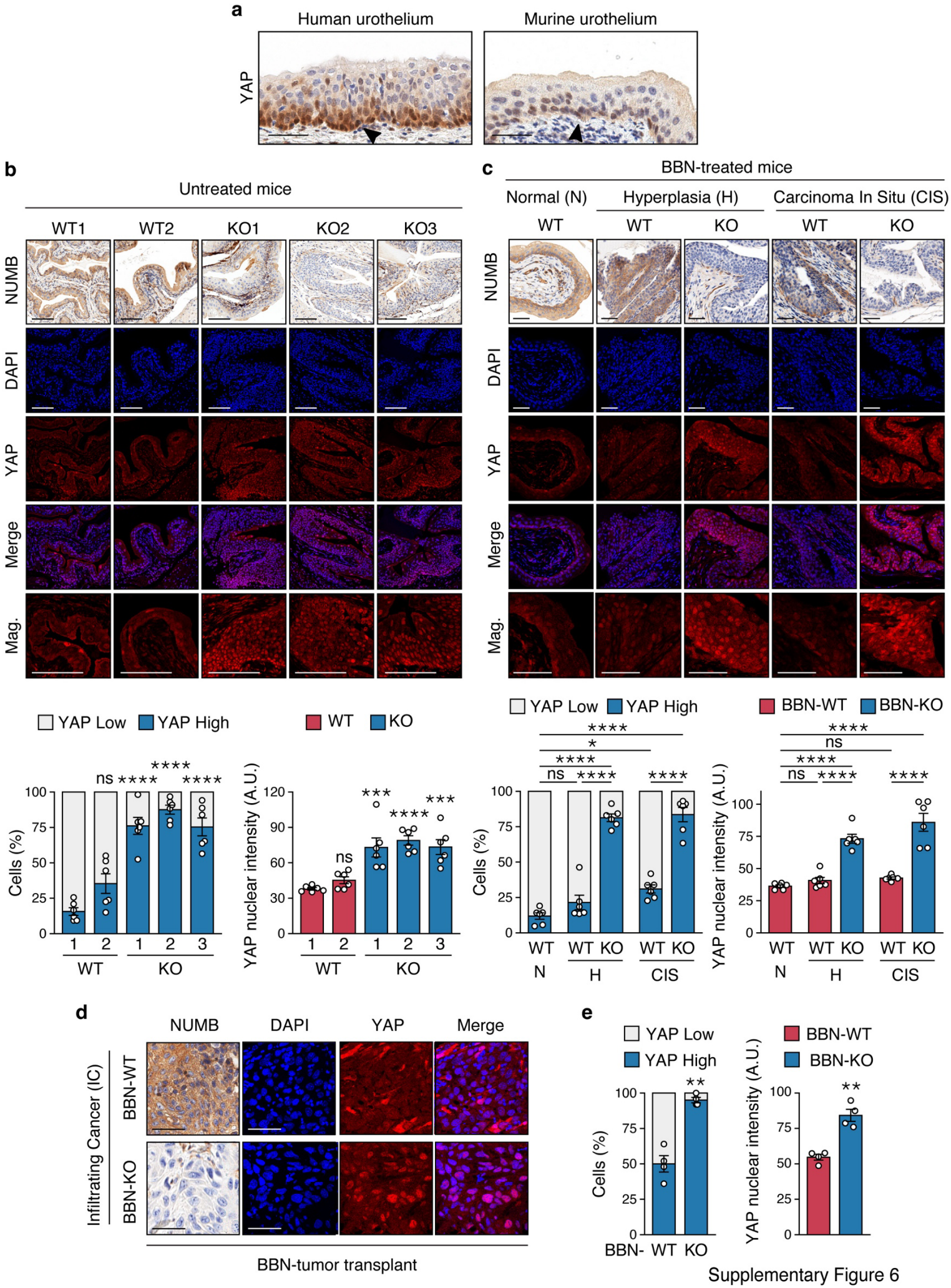
a
Human urothelium
Murine urothelium
YAP
b
Untreated mice
WT1
WT2
KO1
KO2
KO3
NUMB
DAPI
YAP
Merge
Mag.
c
BBN-treated mice
Normal (N)
Hyperplasia (H)
Carcinoma In Situ (CIS)
WT
KO
YAP Low
YAP High
Cells (%)
ns
****
WT
KO
YAP nuclear intensity (A.U.)
***
BBN-WT
BBN-KO
*
N
H
CIS
d
NUMB
DAPI
YAP
Merge
Infiltrating Cancer (IC)
BBN-WT
BBN-KO
BBN-tumor transplant
e
**
BBN-
Supplementary Figure 6

Supplementary Figure 6. NUMB loss is associated with increased nuclear accumulation of YAP in the normal, preneoplastic and overtly neoplastic urothelium. a. Representative IHC images showing the expression pattern of YAP in the normal human and murine urothelium. The black arrowheads point to the basal layer. Bars, 50 μm. **b.** Top, Representative images of bladder tissues obtained from treatment-naïve adult WT (n=2; WT1, WT2) and NUMB-KO (n=3; KO1, KO2, KO3) mice, examined by IHC for NUMB expression and co-stained for YAP (red) and DAPI (blue) by immunofluorescence (IF). Merged images of YAP and DAPI staining and magnifications (Mag.) are shown. Bars, 100 μm. Bottom, Quantification of the % of YAP-high and -low cells and mean nuclear YAP intensity expressed as mean ± SEM, n=6 fields for each condition. ****, $p<0.0001$; ***, $p=0.00046$ for KO1, 0.00041 for KO3; not significant (ns), $p=0.096$ (left), $p=0.85$ (right), *vs.* WT1, by two-sided Tukey's HSD test. **c.** Top, Bladder tissues from 16-week old BBN-treated WT and NUMB-KO mice were examined by IHC for NUMB and co-stained for YAP (red) and DAPI (blue) by IF. Shown are representative images of normal urothelium (N), hyperplasia (H) and carcinoma *in situ* (CIS) detected in a WT bladder, and of hyperplasia (H) and CIS detected in a NUMB-KO bladder. Bars, 50 μm. Bottom, Quantification of the % of YAP- high and -low cells and mean nuclear YAP intensity expressed as mean ± SEM, n=6 fields for each condition. ****, $p<0.0001$; *, $p=0.012$; not significant (ns), $p=0.41$ (left), $p=0.92$ for BBN-WT Hyperplasia *vs.* Normal, $p=0.75$ for BBN-WT CIS *vs.* Normal by two-sided Tukey's HSD test. **d.** Primary infiltrating cancers induced by 20 weeks of BBN treatment in WT and NUMB-KO mice as in 'c' were excised and transplanted into NSG mice. Then, secondary WT and NUMB-KO BBN-tumor transplants (BBN-WT and BBN-KO) were excised and examined by IHC for NUMB and co-stained for YAP (red) and DAPI (blue) by IF. Bars, 50 μm. **e.** Quantification of the experiment in 'd'. Graphs show the % of YAP- high and -low cells and mean nuclear YAP intensity expressed as mean ± SEM, n=4 fields for each condition. **, $p=0.0025$ (left) and 0.0026 (right); by two-sided Welch's t-test *vs.* WT. Source data are provided as Source Data file.

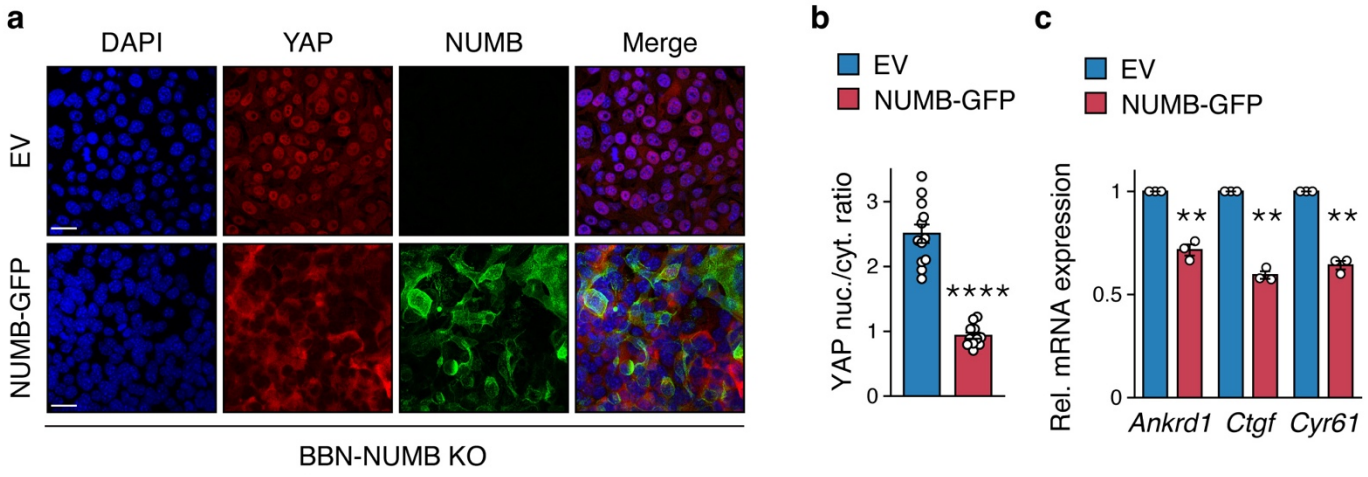

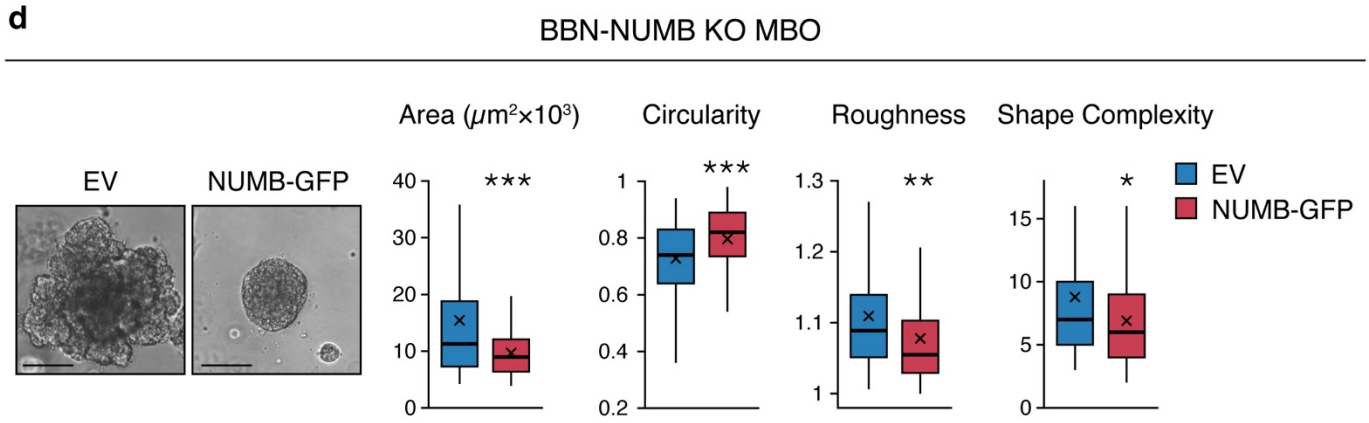

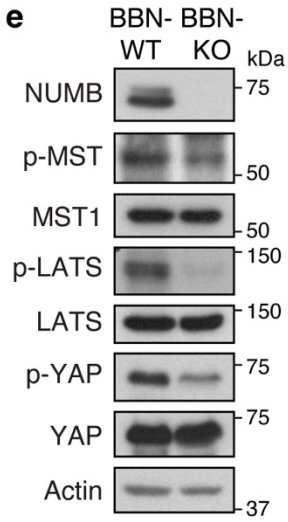

Supplementary Figure 7

Supplementary Figure 7. Restoration of NUMB expression in BBN-KO tumors reverses YAP nuclear accumulation and invasive phenotypes. a. Representative confocal images of BBN-KO tumor cells stably infected with a *NUMB-GFP* lentiviral vector (NUMB-GFP) or an empty vector (EV) and co-stained for endogenous YAP by IF (red) and DAPI (blue). Bar, 25 μm. **b**. Quantification of YAP nuclear/cytoplasmic ratio in cells described in 'a'. Results are reported as the mean ratio/field ± SEM, n=12 fields for each condition from three independent experiments. ****, $p=8.4\times10^{-8}$ by two-sided Welch's t-test *vs.* EV. **c**. RT-qPCR analysis of the indicated YAP transcriptional targets in BBN-KO tumor cells transduced with NUMB-GFP as in 'a'. Graphs show the relative mean fold expression ± SEM from three independent experiments. **, $p=0.009$ for *Ankrd1*, 0.002 for *Ctgf* and 0.0035 for *Cyr61*, by two-sided one-sample t-test. **d**. Representative bright field images and quantitation of morphometric parameters of 3D-Matrigel MBO generated by BBN-KO tumor cells (BBN-NUMB KO MBO), transduced as in 'a'. Graphs show the quantitation of the indicated morphometric parameters (see legend to Fig. 4f). BBN-KO EV, n=79; BBN-KO NUMB-GFP, n=123, obtained from three independent experiments. ***, $p=0.00012$ for Area and 0.00025 for Circularity; **, $p=0.0056$; *, $p=0.04$, by two-sided Welch's t-test *vs.* EV**. e**. Immunoblot analysis of the total and phosphorylated levels of the indicated Hippo pathway components in BBN-WT *vs.* BBN-KO cells. NUMB levels are shown. Actin, loading control. Blot is representative of three independent experiments. Source data are provided as Source Data file.

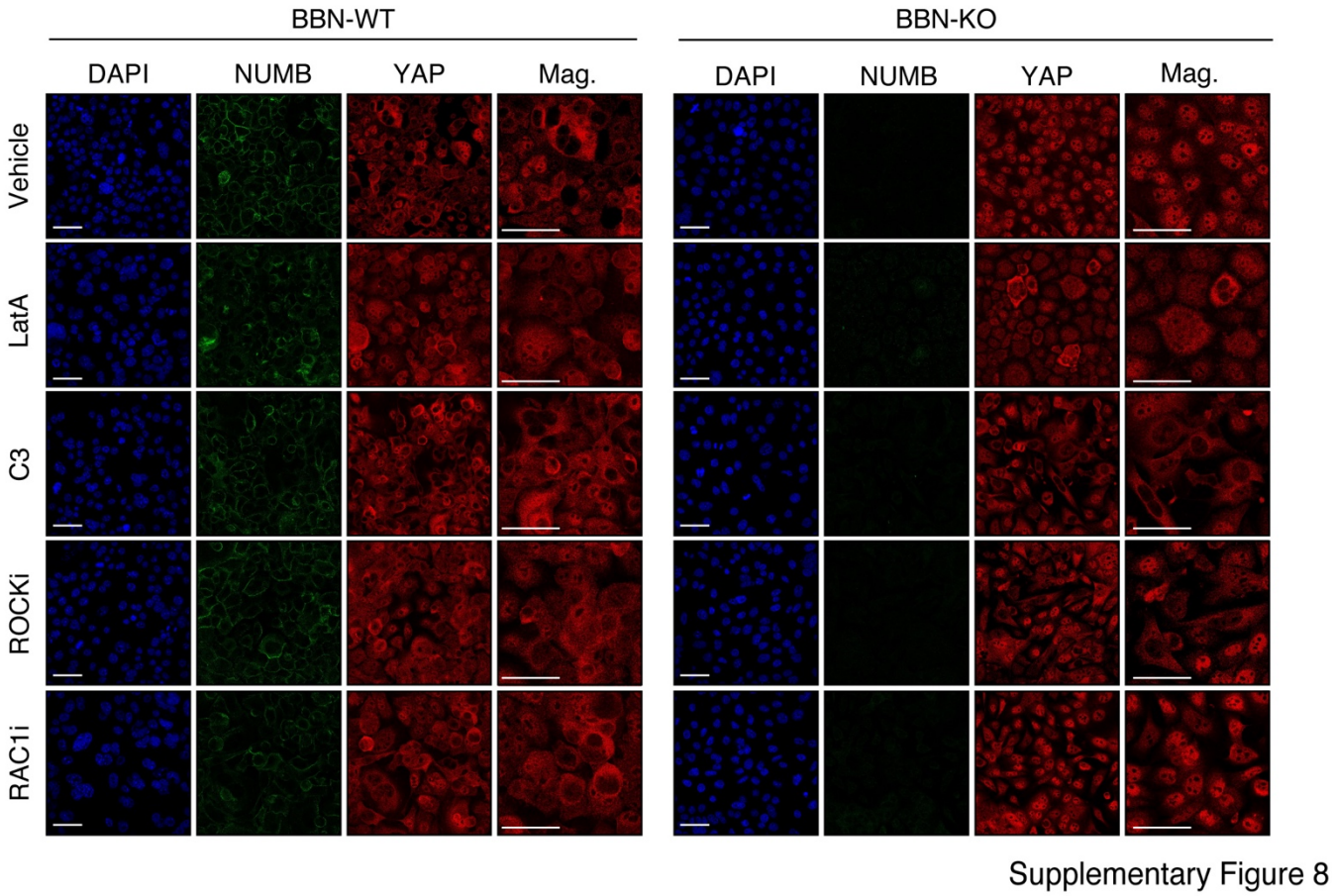

Supplementary Figure 8. **Effects of RHOA, RAC1, ROCK and actin remodeling inhibition on YAP nuclear translocation in BBN-WT and BBN-KO tumor cells.** Representative confocal fluorescence images of BBN-WT and BBN-KO tumor cells treated with the indicated inhibitors (see legend to Fig. 6a) and co-stained for endogenous YAP (red), NUMB (green) and DAPI (blue). A magnification (Mag.) for each condition is shown. Bars, 50 μm.

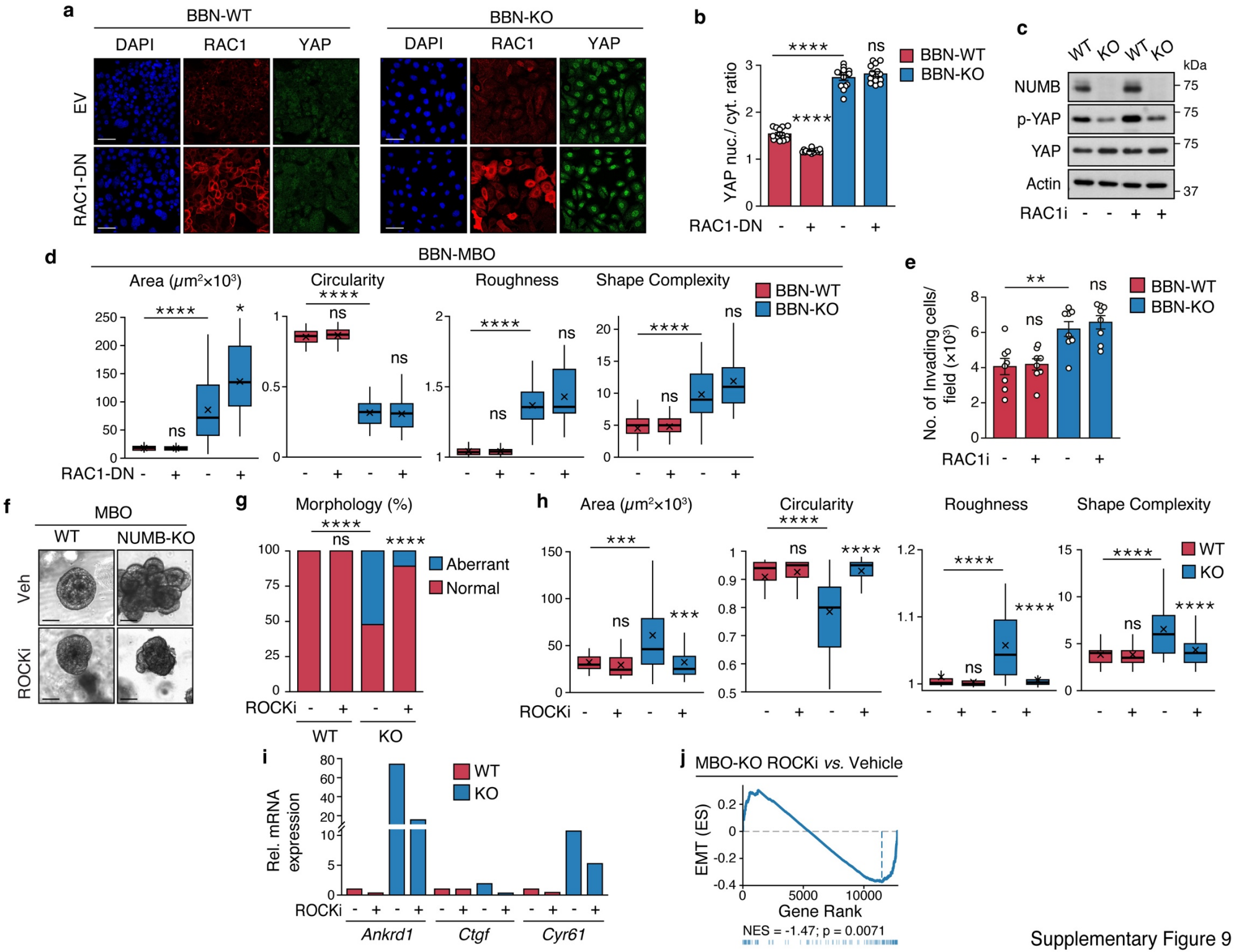

Supplementary Figure 9

Supplementary Figure 9. NUMB loss-induced YAP hyperactivation is insensitive to RAC1 inhibition. a. Representative confocal images of BBN-WT and BBN-KO tumor cells transduced with a lentiviral vector encoding a dominant negative *RAC1* mutant (RAC1-DN) or empty vector (EV) and co-stained for endogenous RAC1 (red), YAP (green) and DAPI (blue). Bar, 50 μm. **b.** Quantification of YAP nuclear/cytoplasmic ratio in cells described in 'a'. Graphs show the mean ± SEM, n=14 fields, from two independent experiments. ****, $p<0.0001$; not significant (ns), $p=0.54$, *vs.* matching controls by two-sided Tukey's HSD test. **c.** Immunoblot analysis of NUMB and total and phosphorylated YAP in BBN-WT and BBN-KO cells treated with the RAC1 inhibitor NSC-23766 (RACi, 10 μM for 12 h). Actin, loading control. Blots shown are representative of two independent experiments. **d.** Analysis of morphometric parameters of BBN-MBO derived from cells treated as described in 'a'. Graphs show the quantitation of the indicated morphometric parameters (see legend to Fig. 4f). BBN-WT EV, n=48; BBN-WT RAC1-DN, n=52; BBN-KO EV, n=37; BBN-KO RAC1-DN, n=19, obtained from two independent experiments. ****, $p<0.0001$; *, $p=0.01$; not significant (ns) p-values are: for BBN-WT cells treated with VP, $p=0.74$ (Area), 0.39 (Circularity), 0.98 (Roughness) and 0.54 (Shape Complexity); for BBN-KO cells treated with VP, $p=0.85$ (Circularity), 0.34 (Roughness) and 0.16 (Shape Complexity), relative to matching condition by FDR-adjusted pairwise two-sided Welch's t-test. **e.** Transwell Matrigel invasion assay of BBN-WT and BBN-KO cells treated with the RAC1 inhibitor, NSC-23766 (RACi, 250 nM for 24 h). Graph shows the average number of invading cells/field calculated 24 h after seeding, expressed as the mean ± SEM of 8 fields from three independent experiments. **, $p=0.006$; not significant (ns), $p=0.83$ for BN-WT and $p=0.61$ for BBN-KO cells treated with RAC1, *vs*. matching controls, by FDR-adjusted pairwise two-sided Welch's t-test. **f.** Representative images of WT and NUMB-KO MBOs grown in 3D-Matrigel in the presence of vehicle (Veh) or ROCK inhibitor Y-27632 (ROCKi, 10μM). Bar, 100 μm. **g.** Frequency of occurrence of normal and aberrant multiacinar morphology in MBO in 'f'. MBO-WT+Veh, n=28; MBO-WT+ROCKi, n=12; MBO-KO+Veh, n=44; MBO-

KO+ROCKi, n=74, obtained from two independent experiments. ****, p<0.0001; not significant (ns), *p*=1, relative to matching condition by FDR-adjusted pairwise two-sided Fisher's t-test. **h.** Analysis of morphometric parameters of MBO in 'f'. Graphs show the quantitation of the indicated morphometric parameters (see also legend to Fig. 4f). MBO-WT+Veh, n=28; MBO-WT+ROCKi, n=12; MBO-KO+Veh, n=44; MBO-KO+ROCKi, n=74, obtained from two independent experiments. ****, *p*<0.0001; ***, *p*=0.00023; not significant (ns) *p*-values are: *p*=0.62 (Area), 0.47 (Circularity), 0.24 (Roughness) and 0.98 (Shape Complexity), relative to matching condition by FDR-adjusted pairwise two-sided Welch's t-test. **i.** Representative RT-qPCR analysis for the indicated YAP transcriptional targets in WT and NUMB-KO MBO treated as in 'f'. Results are reported as the relative mean fold expression from one experiment run in triplicate. **j.** GSEA enrichment plot of the EMT gene signature in NUMB-KO MBO treated as in 'f'. n = 1. ES, Enrichment Score; NES, Normalized Enrichment Score; p, two-sided permutation test p-value. Source data are provided as Source Data file.

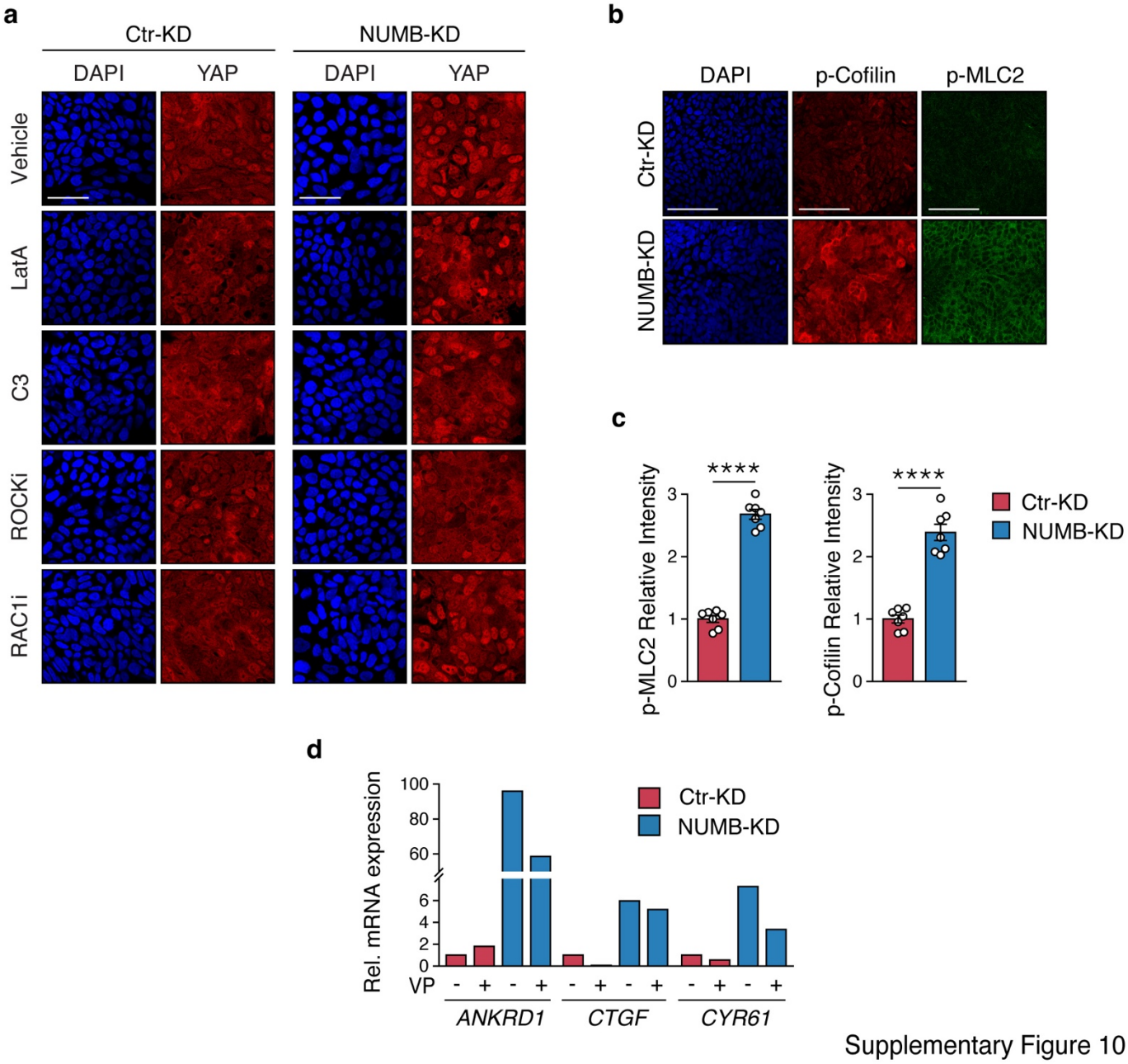

Supplementary Figure 10. NUMB silencing induces increased RHOA/ROCK activity and YAP hyperactivation in human RT4 BCa cells. a. Representative confocal images of Ctr-KD and NUMB-KD RT4 cells treated with the indicated inhibitors (see legend to Fig. 8b) and co-stained for endogenous YAP (red) and DAPI (blue). Bar, 50 µm. **b.** Representative confocal images of Ctr-KD and NUMB-KD RT4 cells co-stained for endogenous phosphorylated cofilin (p-Cofilin, red), phosphorylated MLC2 (p-MLC2, green) and DAPI (blue). Bar, 50 µm. **c.** Quantification of the experiment in 'b' showing the relative intensity of p-MLC2 (left) and p-Cofilin (right) in each condition. Values are the mean/field ± SEM, n=6 fields/condition from one experiment, representative of two independent experiments. ****, $p<0.0001$ by two-sided Welch's t-test *vs.* Ctr-

KD. **d.** Representative RT-qPCR analysis for the indicated YAP transcriptional targets in NUMB-KD and Ctr-KD RT4 cells treated with verteporfin (VP, 3 μM for 8 h) or vehicle-treated. Results are reported as the relative mean fold expression from one experiment run in triplicate. Source data are provided as Source Data file.

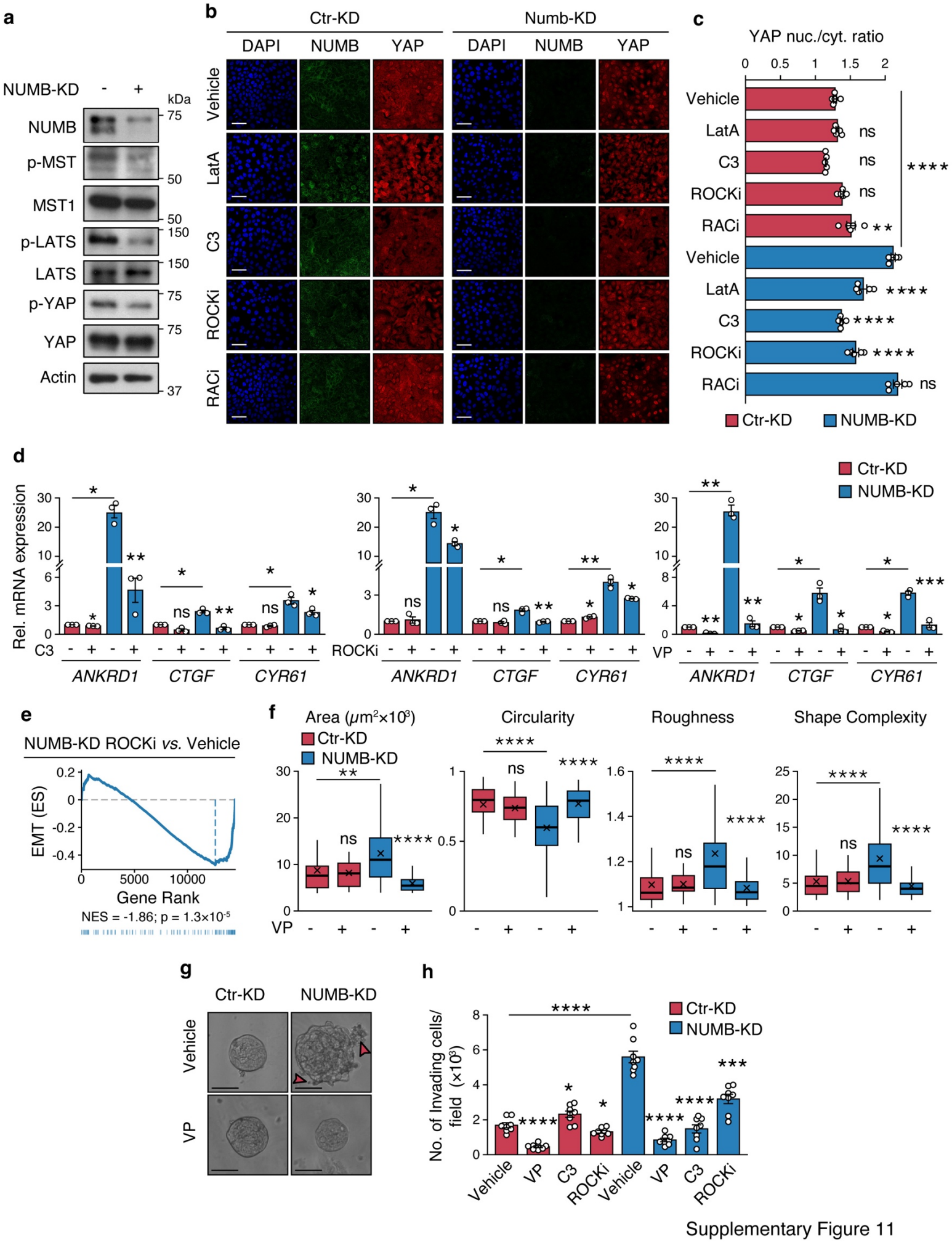

Supplementary Figure 11

Supplementary Figure 11. NUMB silencing induces RHOA/ROCK-dependent YAP hyperactivation in human RT112 BCa cells. a. Immunoblot analysis of NUMB and of the total and phosphorylated levels of the indicated Hippo pathway components in Ctr-KD and NUMB-KD RT112 cells. Actin, loading control. Blots are representative of two independent experiments. **b.** Representative confocal images of Ctr-KD and NUMB-KD RT112 cells treated with the actin polymerization inhibitor latrunculin-A (LatA, 500 nM for 6 h), RHOA inhibitor C3 transferase (C3, 3 μg/ml for 6 h), ROCK inhibitor Y-27632 (ROCKi, 10 μM for 12 h), RAC1 inhibitor, NSC-23766 (RACi, 10 μM for 12 h), or vehicle, and co-stained for endogenous YAP (red), NUMB (green) and DAPI (blue). Bar, 50 μm. **c.** Quantification of the experiment in 'b' showing YAP nuclear/cytoplasmic ratio in the different conditions. Values are the mean/field ± SEM, n=5 fields/condition from one experiment, representative of two independent experiments. ****, $p<0.0001$; **, $p=0.0045$; not significant (ns) *p*-values are: for RT112 Ctr-KD cells treated with LatA, C3, ROKCi, $p=1$, 0.31 and 0.69, respectively, for RT112 NUMB-KD cells treated with RACi, $p=0.97$, relative to matching controls by two-sided Tukey's HSD test. **d.** Representative RT-qPCR analysis for the indicated YAP transcriptional targets in Ctr-KD *vs.* NUMB-KD RT112 cells treated with C3 (3 μg/ml for 6 h) (left), ROCKi (50 μM for 8 h) (middle), verteporfin (VP, 3 μM for 8 h) (right), or vehicle-treated. Graphs show the relative mean fold expression ± SEM from three independent experiments. p-values by FDR-adjusted two-sided one-sample t-test (*vs.* vehicle-treated RT112 Ctr-KD): *ANKRD1*, Ctr-KD C3, $p=0.028$ (*); NUMB-KD Veh, $p=0.023$ (*); *CTGF,* Ctr-KD C3, $p=0.069$ (not significant, ns); NUMB-KD Veh, $p=0.035$ (*); *CYR61*, Ctr-KD C3, $p=0.22$ (ns); NUMB-KD Veh, $p=0.042$ (*) (left); *ANKRD1*, Ctr-KD ROCKi, $p=0.73$ (ns); NUMB-KD Veh, $p=0.014$ (*); *CTGF,* Ctr-KD ROCKi, $p=0.33$ (ns); NUMB-KD Veh, $p=0.047$ (*); *CYR61*, Ctr-KD ROCKi, $p=0.033$ (*); NUMB-KD Veh, $p=0.0097$ (**) (middle); *ANKRD1*, Ctr-KD VP, $p=0.0081$ (**); NUMB-KD Veh, $p=0.0081$ (**); *CTGF,* Ctr-KD VP, $p=0.014$ (*); NUMB-KD Veh, $p=0.0.37$ (*); *CYR61*, Ctr-KD VP, $p=0.019$ (*); NUMB-KD Veh, $p=0.011$ (*) (right). p-values by FDR-adjusted two-sided Welch's t-test: C3- *vs.* vehicle-treated NUMB-KD (left), *ANKRD1*, $p=0.0026$

(**); *CTGF*, p=0.001 (**); *CYR61*, p=0.049 (*); ROCKi- *vs.* vehicle-treated NUMB-KD (middle): *ANKRD1*, p=0.026 (*); *CTGF*, p=0.0089 (**); *CYR61*, p=0.034 (*); VP- *vs.* vehicle-treated NUMB-KD (right): *ANKRD1*, p=0.004 (**); *CTGF*, p=0.015 (*); *CYR61*, p=0.00079 (***). **e.** GSEA enrichment plot of the EMT gene signature in RT112 NUMB-KD cells treated with ROCKi, as in 'd', *vs.* vehicle. n = 1. ES, Enrichment Score; NES, Normalized Enrichment Score; p, two-sided permutation test p-value. **f.** Analysis of morphometric parameters in 3D-Matrigel organoids derived from Ctr-KD and NUMB-KD RT112 cells treated with VP (25 nM) or vehicle. Graphs show the quantitation of the indicated morphometric parameters (see legend to Fig. 4f). Ctr-KD+Vehicle, n=32; Ctr-KD+VP, n=35; NUMB-KD+Vehicle, n=133; NUMB+VP, n=57, obtained from two independent experiments. ****, p<0.0001; **, p=0.003; not significant (ns) p-values are: p=0.61, 0.51, 0.89 and 0.96 for Area, Circularity, Roughness and Shape Complexity, respectively, relative to matching condition by FDR-adjusted pairwise two-sided Welch's t-test. **g.** Representative bright field images of stable NUMB-KD *vs.* Ctr-KD RT112 organoids in 'f'. Red arrowheads point to invasive protrusions. Bar, 50 μm. **h.** Transwell Matrigel invasion assay of Ctr-KD and NUMB-KD RT112 cells treated for 24 h with VP (100 nM), C3 (3 μg/mL), Y-27632 (10 μM) or vehicle. Graph shows the average number of invading cells/field in each condition expressed as the mean ± SEM of 8 fields from two independent experiments. ****, p<0.0001, ***, p=0.00017; *, p=0.021 and 0.045 for RT112 Ctr-KD cells treated with C3 and ROCKi, respectively, relative to matching controls by FDR-adjusted pairwise two-sided Welch's t-test. Source data are provided as Source Data file.

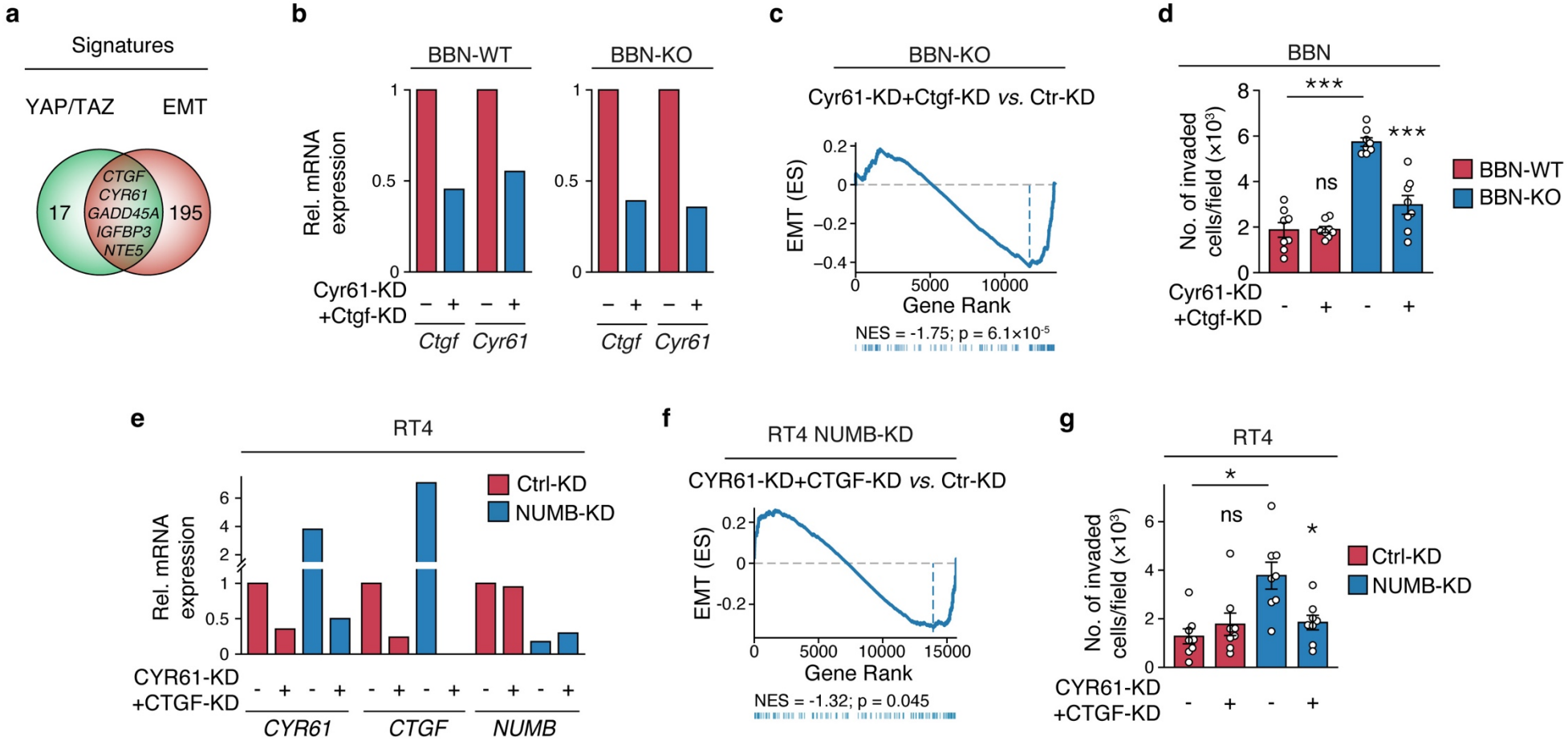

Supplementary Figure 12

Supplementary Figure 12. Direct involvement of the YAP transcriptional targets CYR61 and CTGF in EMT activation.

a. Venn diagram showing the overlap between the 22-gene YAP signature and the 200 genes of the EMT gene signature from the Hallmark MSigDB. **b.** Representative RT-qPCR analysis of *Cyr61* and *Ctgf* in BBN-WT and BBN-KO cells lentivirally transduced with a shRNA targeting luciferase as a control (-) or simultaneously silenced for *Cyr61* and *Ctgf* (*Cyr61*-KD+*Ctgf*-KD). Results are reported as the relative mean fold expression from one experiment run in triplicate. **c.** GSEA enrichment plot of the EMT gene signature in *Cyr61*-KD+*Ctgf*-KD *vs.* Ctr-KD BBN-KO cells treated as in 'b'. n=1. ES, Enrichment Score; NES, Normalized Enrichment Score; p, two-sided permutation test p-value. **d.** Transwell Matrigel invasion assay of BBN-WT and BBN-KO cells lentivirally transduced with a shRNA targeting luciferase as a control (-) or simultaneously silenced for *Cyr61* and *Ctgf* (*Cyr61*-KD+*Ctgf*-KD). Graph shows the average number of invading cells/field in each condition expressed as the mean ± SEM of 8 fields from two independent experiments. ****, $p<0.0001$; ***, $p=0.00027$; not significant (ns), $p=0.89$, relative to matching controls by FDR-adjusted pairwise two-sided Welch's t-test. **e.** Representative RT-qPCR analysis for *CYR61*, *CTGF* and *NUMB* in NUMB-KD and Ctr-KD RT4 cells simultaneously silenced for *CYR6* and *CTGF* (CYR61-KD+CTGF-KD) *vs.* control-silenced (Ctr-KD). Results are reported as the relative mean fold expression from one experiment run in triplicate. **f.** GSEA enrichment plot of the EMT gene signature in CYR61-KD+CTGF-KD *vs.* Ctr-KD NUMB-KD RT4 cells. n = 1. ES, Enrichment Score; NES, Normalized Enrichment Score; p, two-sided permutation test p-value. **g.** Transwell Matrigel invasion assay of Ctr-KD and NUMB-KD RT4 cells silenced for *CYR61+CTGF vs.* control-silenced. Graph shows the average number of invading cells/field in each condition expressed as the mean ± SEM of 8 fields from two independent experiments. *, $p=0.014$ and 0.03 for RT4 NUMB-KD cells control-silenced and *CYR61+CTGF* silenced, respectively; not significant (ns), $p=0.46$, relative to matching controls by FDR-adjusted pairwise two-sided Welch's t-test. Source data are provided as Source Data file

SUPPLEMENTARY TABLES AND LEGENDS

Factor		Numb		Total	OR (95% CI)	p-value
		High	Low			
Sex	Female	51 (73.9%)	18 (26.1%)	69	Ref.	
	Male	225 (78.4%)	62 (21.6%)	287	0.78 (0.4 - 1.5)	0.42
Age	≤ 70	152 (76.8%)	46 (23.2%)	198	Ref.	
	> 70	124 (78.5%)	34 (21.5%)	158	0.91 (0.5 - 1.5)	0.8
Tumor Extension	pTa/CIS/pT1	46 (88.5%)	6 (11.5%)	52	Ref.	
	pT2	39 (78%)	11 (22%)	50	2.12 (0.7 - 6.8)	0.19
	pT3	128 (76.6%)	39 (23.4%)	167	2.28 (1.0 - 6.4)	0.077
	pT4	63 (72.4%)	24 (27.6%)	87	2.85 (1.1 - 8.3)	0.033
Lymp Node Status	pN0	164 (81.6%)	37 (18.4%)	201	Ref.	
	pN+	102 (71.3%)	41 (28.7%)	143	1.78 (1.1 - 3.0)	0.027
	pNX	10 (83.3%)	2 (16.7%)	12	0.94 (0.1 - 3.8)	1
Vascular Invasion	Absent	167 (81.5%)	38 (18.5%)	205	Ref.	
	Present	109 (72.2%)	42 (27.8%)	151	1.69 (1.0 - 2.8)	0.041
Total		276 (77.5%)	80 (22.5%)	356		

Supplementary Table 1. Association between clinicopathological variables and NUMB IHC status (High vs. Low) in the retrospective longitudinal cohort of 356 post-cystectomy MIBC patients. OR (95% CI), Odds Ratio (95% Confidence Interval); p-value, two-sided Fisher's exact test p-value.

Factor		NUMB		Total	OR (95% CI)	p-value
		High	Low			
Sex	Female	7 (58.3%)	5 (41.7%)	12	Ref.	
	Male	52 (80%)	13 (20%)	65	0.35 (0.1 - 1.4)	0.14
Age		73.1±9.6	75.2±7.8			0.34
Tumor Extension	pTa/CIS	27 (81.8%)	6 (18.2%)	33	Ref.	
	pT1	32 (72.7%)	12 (27.3%)	44	1.66 (0.6 - 5.4)	0.42
Total		59 (76.6%)	18 (23.4%)	77		

Supplementary Table 2. Association between clinicopathological variables and NUMB IHC status (High vs. Low) in a retrospective longitudinal cohort of 77 NMIBC patients; p-value, two-sided Fisher's exact test p-value for categorical variables and two-sided Welch's t-test for Age.

Factor		NUMB		Total	OR (95% CI)	p-value
		High	Low			
Sex	Male	222 (53.6%)	192 (46.4%)	414	Ref.	
	Female	59 (48.8%)	62 (51.2%)	121	1.21 (0.8 - 1.8)	0.35
Age		68.4±11.2	68±10.4			0.65
Grade	Low	173 (54.1%)	147 (45.9%)	320	Ref.	
	High	108 (50.2%)	107 (49.8%)	215	1.17 (0.8 - 1.6)	0.43
Tumor Extension	pTa	191 (54.3%)	161 (45.7%)	352	Ref.	
	CIS	24 (50%)	24 (50%)	48	1.19 (0.6 - 2.2)	0.64
	pT1	66 (48.9%)	69 (51.1%)	135	1.24 (0.8 - 1.8)	0.31
Therapy	No	121 (54.3%)	102 (45.7%)	223	Ref.	
	Yes	157 (53.2%)	138 (46.8%)	295	1.04 (0.7 - 1.5)	0.86
	Unknown	3 (17.6%)	14 (82.4%)	17	5.29 (1.6 - 24.5)	0.0046
Total		281 (52.5%)	254 (47.5%)	535		

Supplementary Table 3. Association between clinicopathological variables and NUMB^{LESS} status (Like vs. Not-like) in the 535 NMIBC patients of the UROMOL cohort; p-value, two-sided Fisher's exact test p-value for categorical variables and two-sided Welch's t-test for Age.

Cancer Hallmark	NES	p-value	Adjusted p-value
OXIDATIVE PHOSPHORYLATION	-1.76	8.00E-07	4.00E-05
EPITHELIAL MESENCHYMAL TRANSITION	1.62	5.13E-05	0.0013
MYOGENESIS	1.49	0.0016	0.025
UV RESPONSE DN	1.48	0.0027	0.025
MYC TARGETS V2	-1.69	0.0029	0.025
APICAL JUNCTION	1.45	0.0030	0.025

Supplementary Table 4. Significantly enriched "MSigDB Hallmark" gene signatures in RNA-Seq of MIBC Numb^{Low} (HT1376, CLS439, 5637) *vs.* NMIBC Numb^{High} BC (KK47, RT4, RT112) cell lines by GSEA. p-value, two-sided permutation test p-value; Adjusted p-value, FDR adjusted p-value.

Cancer Hallmark	NES	p-value	Adjusted p-value
OXIDATIVE PHOSPHORYLATION	-1.96	2.16E-08	1.08E-06
MTORC1 SIGNALING	-1.89	1.31E-07	3.27E-06
MYC TARGETS V1	-1.88	2.97E-07	4.95E-06
UNFOLDED PROTEIN RESPONSE	-1.86	2.00E-05	0.00025
UV RESPONSE DN	1.75	0.00022	0.0022
HYPOXIA	-1.62	0.00041	0.0034
MYC TARGETS V2	-1.78	0.00054	0.0038
GLYCOLYSIS	-1.60	0.00065	0.0041
ADIPOGENESIS	-1.56	0.0017	0.0094
INTERFERON ALPHA RESPONSE	-1.61	0.0022	0.010
ESTROGEN RESPONSE LATE	-1.55	0.0023	0.010
P53 PATHWAY	-1.49	0.0040	0.017
INTERFERON GAMMA RESPONSE	-1.52	0.0050	0.019
ANGIOGENESIS	1.71	0.0066	0.024
APICAL JUNCTION	1.49	0.011	0.036
ALLOGRAFT REJECTION	-1.51	0.012	0.036
ESTROGEN RESPONSE EARLY	-1.44	0.014	0.041
EPITHELIAL MESENCHYMAL TRANSITION	1.45	0.015	0.041
COMPLEMENT	-1.42	0.018	0.048

Supplementary Table 5. Significantly enriched "MSigDB Hallmark" gene signatures in RNA-Seq of RT4 Numb-KD *vs.* Ctr-KD cell lines by GSEA. NES, Normalized Enriched Score; p-value, two-sided permutation test p-value; Adjusted p-value, FDR adjusted p-value.

Cancer Hallmark	NES	p-value	Adjusted p-value
EPITHELIAL MESENCHYMAL TRANSITION	1.98	1.18E-06	5.89E-05
INTERFERON ALPHA RESPONSE	2.01	6.74E-05	0.0017
INTERFERON GAMMA RESPONSE	1.72	0.00036	0.0061
UV RESPONSE DN	1.72	0.00049	0.0061
IL6 JAK STAT3 SIGNALING	-1.75	0.00076	0.0076
P53 PATHWAY	-1.57	0.0010	0.0076
ESTROGEN RESPONSE EARLY	-1.56	0.0011	0.0076
ESTROGEN RESPONSE LATE	-1.53	0.0018	0.011
HEME METABOLISM	-1.51	0.0030	0.016
APICAL SURFACE	-1.69	0.0031	0.016
CHOLESTEROL HOMEOSTASIS	-1.60	0.0048	0.021
E2F TARGETS	1.53	0.0051	0.021
MTORC1 SIGNALING	-1.43	0.0071	0.027
GLYCOLYSIS	-1.42	0.0089	0.032
UV RESPONSE UP	-1.44	0.014	0.047

Supplementary Table 6. Significantly enriched "MSigDB Hallmark" gene signatures in RNA-Seq of RT112 Numb-KD *vs.* Ctr-KD cell lines by GSEA. NES, Normalized Enriched Score; p-value, two-sided permutation test p-value; Adjusted p-value, FDR adjusted p-value.

Cancer Hallmark	NES	p-value	Adjusted p-value
EPITHELIAL MESENCHYMAL TRANSITION	2.04	1.47E-07	7.36E-06
UNFOLDED PROTEIN RESPONSE	-1.8	0.0005	0.0092
MYC TARGETS V1	-1.61	0.0006	0.0092
IL6 JAK STAT3 SIGNALING	-1.82	0.00088	0.0092
HEME METABOLISM	-1.6	0.00099	0.0092
E2F TARGETS	-1.58	0.0011	0.0092
HYPOXIA	1.59	0.0014	0.0099
APICAL JUNCTION	1.59	0.0022	0.014
COAGULATION	1.66	0.005	0.025
INTERFERON GAMMA RESPONSE	-1.49	0.005	0.025
UV RESPONSE DN	1.53	0.0068	0.031
G2M CHECKPOINT	-1.45	0.0074	0.031
GLYCOLYSIS	1.47	0.01	0.039
MTORC1 SIGNALING	-1.37	0.012	0.042
KRAS SIGNALING UP	1.52	0.014	0.047

Supplementary Table 7. Significantly enriched "MSigDB Hallmark" gene signatures in RNA-Seq of KK47 Numb-KD *vs.* Ctr-KD cell lines by GSEA. NES, Normalized Enriched Score; p-value, two-sided permutation test p-value; Adjusted p-value, FDR adjusted p-value.

Structure	Histology	NUMB$^{lox/lox}$ CK5-Cre			CK5-Cre		
		≤ 24 weeks	> 24 weeks	Total	≤ 24 weeks	> 24 weeks	Total
Bladder	Normal	2	1	33.3% (3/9)	3	4	63.6% (7/11)
	Hyperplasia	2	2	44.4% (4/9)	3	1	36.4% (4/11)
	CIS	1	1	22.2% (2/9)	0	0	0% (0/11)
Breast	Normal	4	1	100% (5/5)	5	3	100% (8/8)
	Not eval.	1	3	(4)	1	2	(3)
Broncus	Normal	5	4	100% (9/9)	6	5	100% (11/11)
Deferent Duct	Normal	5	4	100% (9/9)	6	5	100% (11/11)
Esophagus	Normal	5	3	100% (8/8)	6	5	100% (8/11)
	Not eval.		1	(1)	1	2	(3)
Kidney	Normal	5	4	100% (9/9)	6	5	100% (11/11)
Lung	Normal	5	4	100% (9/9)	6	5	100% (11/11)
Oral Mucosa	Normal	5	4	100% (9/9)	6	5	100% (11/11)
Prostate	Normal	5	4	100% (9/9)	6	5	100% (11/11)
Salivary Gland	Normal	5	4	100% (9/9)	6	5	100% (11/11)
Seminal Vescicle	Normal	5	4	100% (9/9)	6	5	100% (11/11)
Skin	Normal	5	4	100% (9/9)	6	5	100% (11/11)
Tongue	Normal	5	4	100% (9/9)	6	5	100% (11/11)
Ureter	Normal	5	4	100% (9/9)	6	5	100% (11/11)
No. of mice		5	4	9	6	5	11

Supplementary Table 8. Frequency of histological phenotypes observed in CK5-positive tissues analyzed in age-matched male NUMB-KO (Numb$^{lox/lox}$ Ck5-CRE) and NUMB-WT (Ck5-CRE) mice sacrificed at different weeks of age. Not eval., not evaluable.

Cancer Hallmark	NES	p-value	Adjusted p-value
HYPOXIA	1.97	1.55E-07	7.75E-06
G2M CHECKPOINT	1.87	5.72E-06	0.00014
INTERFERON ALPHA RESPONSE	1.76	0.00055	0.009
EPITHELIAL MESENCHYMAL TRANSITION	1.67	0.00098	0.012
TNFA SIGNALING VIA NFKB	1.63	0.0015	0.015
INTERFERON GAMMA RESPONSE	1.59	0.0019	0.016
INFLAMMATORY RESPONSE	1.61	0.0025	0.018
ESTROGEN RESPONSE LATE	1.48	0.0076	0.047

Supplementary Table 9. Significantly enriched "MSigDB Hallmark" gene signatures in RNA-Seq of NUMB-KO *vs.* WT MBO by GSEA. NES, Normalized Enriched Score; p-value, two-sided permutation test p-value; Adjusted p-value, FDR adjusted p-value.

Cancer Hallmark	NES	p-value	Adjusted p-value
XENOBIOTIC METABOLISM	-2.06	1.33E-08	6.64E-07
EPITHELIAL MESENCHYMAL TRANSITION	2.00	5.59E-08	1.40E-06
INTERFERON ALPHA RESPONSE	-1.95	3.15E-05	0.00052
ESTROGEN RESPONSE LATE	-1.71	4.51E-05	0.00056
P53 PATHWAY	-1.60	0.0002	0.002
ADIPOGENESIS	-1.60	0.0003	0.0025
BILE ACID METABOLISM	-1.72	0.0012	0.0086
INTERFERON GAMMA RESPONSE	-1.54	0.0016	0.010
FATTY ACID METABOLISM	-1.60	0.0025	0.014
ESTROGEN RESPONSE EARLY	-1.42	0.0055	0.027
ANGIOGENESIS	1.73	0.0060	0.027
PEROXISOME	-1.58	0.010	0.043

Supplementary Table 10. Significantly enriched "MSigDB Hallmark" gene signatures in RNA-Seq of BBN-KO *vs.* BBN-WT tumor cells by GSEA. NES, Normalized Enriched Score; p-value, two-sided permutation test p-value; Adjusted p-value, FDR adjusted p-value.